Impact of interface stiffness in surface-wave resonances on nanostrip-attached substrates

Hirotsugu Ogi,* Shoichi Masuda, Akira Nagakubo, Nobutomo Nakamura, and Masahiko Hirao
Graduate School of Engineering Science, Osaka University, Toyonaka, Osaka 560-8531, Japan

Kouta Kondou† and Teruo Ono
Institute for Chemical Research, Kyoto University, Gokasho, Uji, Kyoto 611-0011, Japan
(Received 4 November 2015; revised manuscript received 18 December 2015; published 22 January 2016)

Surface waves are often excited by interdigitated transducers consisting of many nanostrips attached on a substrate, and it has been recognized that the mass and stiffness of the attached nanostrips affect surface-wave resonances to some extent. Here, we reveal the more noticeable influence of the interfacial stiffness between strips and substrate at high frequencies. This influence is confirmed by exciting and detecting surface-wave resonances up to ~ 6 GHz by picosecond ultrasound spectroscopy. The resonance frequency significantly decreases and attenuation increases as the interfacial stiffness decreases for silicon substrate. However, low-attenuation branches appear along the Rayleigh-wave-resonance dispersion curve for silica substrate, and the resonance frequencies remain nearly identical to those of the Rayleigh waves. Previous models fail to reproduce these surface-wave resonance behaviors. The proposed theoretical model, involving the interfacial stiffness, consistently explained them, indicating the importance of the interface bond strength in designing surface-wave resonators.

DOI: 10.1103/PhysRevB.93.024112

I. INTRODUCTION

Surface-wave propagation on periodically modified structures has been intensively studied [1–4] because of its relevance to acoustic resonators, where interdigitated-transducer electrodes, composed of many metallic nanostrips, are attached on surfaces to excite and detect surface-wave resonances. Glass *et al.* proposed a theoretical model for surface waves propagating on a grating surface of arbitrary periodic profiles [5] and expanded its analysis for leaky surface waves [6]. Yantchev *et al.* [7] theoretically studied interaction between surface waves and Lamb modes for a plate with metallic strips on its surface and found the coexistence of two independent eigenmodes associated by the periodic grating. Maznev and Every [8] analyzed the periodic mass-loading effect on a soft thin layer on the substrate surface and found some important surface-wave propagation behaviors, including a large band gap inside the Brillouin zone caused by the hybridization of the Rayleigh and Sezawa modes.

Despite the numerous studies on surface-wave propagation behaviors, the influence of the bond strength at the interface between deposited strips and the substrate surface was less studied, and we here reveal that it significantly affects the sound velocity and attenuation of leaky surface waves at high frequencies. Because operating frequencies of surface-wave-resonator devices are being raised due to lack of a communication frequency band, this result poses a highly practical impact as well. Using picosecond ultrasound spectroscopy [9–12], we measure surface-wave resonance frequencies on substrates on which copper nanostrips are attached. The surface-wave resonance frequency is significantly lower than the Rayleigh-wave resonance frequency on silicon substrate, regardless of the much smaller thickness of the attached strips than the wavelength. On the other hand, it is identical to the Rayleigh-wave resonance frequency on silica substrate. Previous theoretical models fail to reproduce these observations, and we propose an alternative model considering the interfacial stiffness as well as the mass-loading effect. Our theoretical calculation consistently explains these resonance behaviors, demonstrating that the bond strength at the interface dominates the resonance frequency and attenuation of surface waves at high frequencies.

II. THEORY

The two-dimensional space of the x_1-x_3 plane is considered. The half space of $x_3 > 0$ defines an isotropic substrate, and the strips are connected with elastic springs. (We regarded the Si substrate as an isotropic material for simplicity and used aggregated elastic constants $C_{11} = 184.5$ GPa and $C_{44} = 66.24$ GPa. For silica, we used $C_{11} = 73.8$ GPa and $C_{44} = 25.0$ GPa.) The spring constants per unit area along in-plane and out-of-plane directions are denoted as K_1 and K_3, respectively (Fig. 1). Because the surface waves originate from the strips, displacements in the substrate, u_1 and u_3, can be expressed by superimposing partial waves with in-plane Bloch-harmonics wave numbers k_1^n ($n = 0, \pm1, \pm2,...$) [6,8,13]:

$$u_1 = \sum_n \left\{ A_n k_1^n e^{i(k_1^n x_1 + k_3^{Ln} x_3 - \omega t)} + B_n k_3^{Sn} e^{i(k_1^n x_1 + k_3^{Sn} - \omega t)} \right\}, \quad (1)$$

$$u_3 = \sum_n \left\{ A_n k_3^{Ln} e^{i(k_1^n x_1 + k_3^{Ln} x_3 - \omega t)} - B_n k_1^n e^{i(k_1^n x_1 + k_3^{Sn} - \omega t)} \right\}. \quad (2)$$

Here,

$$k_1^n = k_1 + \frac{2\pi n}{d}, \quad (3)$$

and k_3^{Ln} and k_3^{Sn} are corresponding wave numbers along the x_3 direction for longitudinal and shear waves, respectively, given

*ogi@me.es.osaka-u.ac.jp
†Present address: Center for Emergent Matter Science, Riken, 2-1 Hirosawa, Wako, Saitama 351-0198 Japan.

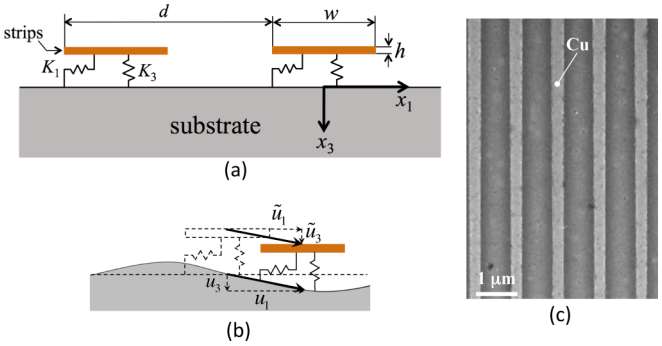

FIG. 1. (a) Two-dimensional model with interface spring constants, (b) displacements of nanostrips and those in substrate, and (c) scanning-electron-microscopy image for nanostrip lines with period $d = 1000$ nm fabricated on the silicon substrate.

by

$$k_3^{\mathrm{L,S}n} = \begin{cases} i\sqrt{\left(k_1^n\right)^2 - \frac{\omega^2}{(C_{\mathrm{L,S}})^2}}, & \left(k_1^n\right)^2 > \frac{\omega^2}{(C_{\mathrm{L,S}})^2}, \\ \sqrt{\frac{\omega^2}{(C_{\mathrm{L,S}})^2} - \left(k_1^n\right)^2}, & \left(k_1^n\right)^2 < \frac{\omega^2}{(C_{\mathrm{L,S}})^2}. \end{cases} \tag{4}$$

$C_{\mathrm{L,S}}$ means longitudinal-wave (C_{L}) or shear-wave (C_{S}) velocity in the substrate. Because the displacements of strip (denoted by $\tilde{u}_1$ and $\tilde{u}_3$) arise, responding to the surface deformation, they are also expanded with Bloch-harmonics terms:

$$\tilde{u}_1 = \sum_n C_n k_1^n \mathrm{e}^{i(k_1^n x_1 - \omega t)}, \quad \tilde{u}_3 = \sum_n D_n k_1^n \mathrm{e}^{i(k_1^n x_1 - \omega t)}. \tag{5}$$

There are two kinds of boundary conditions. First is the balance between the stress and spring force on the substrate surface:

$$\rho C_{\mathrm{S}}^2 \left(\frac{\partial u_1}{\partial x_3} + \frac{\partial u_3}{\partial x_1} \right) - K_1(u_1 - \tilde{u}_1) = 0, \tag{6}$$

$$\rho\left(C_{\mathrm{L}}^2 - 2C_{\mathrm{S}}^2\right)\frac{\partial u_1}{\partial x_1} + \rho C_{\mathrm{L}}^2 \frac{\partial u_3}{\partial x_3} - K_3(u_3 - \tilde{u}_3) = 0, \tag{7}$$

where ρ denotes the mass density of the substrate. Second is the balance between the inertia force and spring force at the strip:

$$\rho_s(x_1)\frac{\partial^2 \tilde{u}_j}{\partial t^2} + K_j(\tilde{u}_j - u_j), \quad j = 1,3. \tag{8}$$

Here, $\rho_s(x_1)$ expresses the area mass density for the attached strips, and it can be expanded with the Bloch-harmonics components as [7]

$$\rho_s(x_1) = \sum_{n=-\infty}^{\infty} \rho_s^n \exp\left(i\frac{2\pi n}{d} x_1 \right), \tag{9}$$

where

$$\rho_s^n = \rho h \times \begin{cases} \frac{1}{\pi n}\sin\left(\frac{\pi n w}{d}\right), & n \neq 0 \\ \frac{w}{d}, & n = 0. \end{cases} \tag{10}$$

Here, h and w are height and width of the strip, respectively. Substituting the displacements [Eqs. (1), (2), and (5)] and mass distribution [Eq. (9)] into the boundary conditions [Eqs. (6)–(8)], we obtain linear equations for individual n values:

$$\left(2ik_1^n k_3^{\mathrm{L}n} - \frac{K_1 k_1^n}{\rho C_{\mathrm{S}}^2}\right)A_n + \left[i\left\{\left(k_3^{\mathrm{S}n}\right)^2 - \left(k_1^n\right)^2\right\} - \frac{K_1 k_3^{\mathrm{S}n}}{\rho C_{\mathrm{S}}^2}\right]B_n + \left(\frac{K_1}{\rho C_{\mathrm{S}}^2}\right)C_n = 0, \tag{11}$$

$$\left[i\left\{\frac{\omega^2}{C_{\mathrm{S}}^2} - 2\left(k_1^n\right)^2\right\} - \frac{K_3 k_3^{\mathrm{L}n}}{\rho C_{\mathrm{S}}^2}\right]A_n + \left(-2ik_1^n k_3^{\mathrm{S}n} + \frac{K_3 k_1^n}{\rho C_{\mathrm{S}}^2}\right)B_n + \left(\frac{K_3}{\rho C_{\mathrm{S}}^2}\right)D_n = 0, \tag{12}$$

$$K_1 k_1^n A_n + K_1 k_3^{\mathrm{S}n} B_n - K_1 C_n + \omega^2 \sum_{m=-\infty}^{\infty} \rho_s^{n-m} C_m = 0, \tag{13}$$

$$K_3 k_3^{\mathrm{L}n} A_n - K_3 k_1^n B_n - K_3 D_n + \omega^2 \sum_{m=-\infty}^{\infty} \rho_s^{n-m} D_m = 0. \tag{14}$$

For obtaining meaningful solutions for nonzero coefficients A_n, B_n, C_n, and D_n, the determinant of the matrix constructed by the system of equations [Eqs. (11)–(14)] should be zero, yielding the frequency equation. A careful concern has been paid for defining the complex wave numbers $k_3^{\mathrm{L,S}n}$ in Eq. (4). Leaky surface waves, possessing positive imaginary parts in $k_1^n[\mathrm{Im}(k_1^n) > 0]$, radiate bulk waves propagating toward inside the substrate, whose wave numbers $k_3^{\mathrm{L,S}n}$ show positive real parts. Because the imaginary part of $(k_3^{\mathrm{L,S}n})^2$, which equals $-2\mathrm{Re}(k_1^n)\mathrm{Im}(k_1^n)$, must be negative for positive k_1 and n values, imaginary parts of $k_3^{\mathrm{L,S}n}$ should be negative, implying exponentially increasing amplitude with increase in x_3. This is, however, physically correct as discussed previously [6]. The demand $\mathrm{Im}(k_1^n) > 0$ for leaky surface waves accepts the infinite surface-wave amplitude at $x_1 \to -\infty$, and the bulk wave radiated from the source at $x_1 \to -\infty$ shows the infinite amplitude, where x_3 becomes infinity at a finite time.

We solved the frequency equation for a given real part of the surface-wave wave number $\mathrm{Re}(k_1)$, seeking the frequency w and the imaginary part of the wave number, the latter of which corresponds to attenuation of leaky surface waves. Contributions of partial plane waves becomes less significant as n and m increase, and we find that involving components up to 10 gave sufficiently convergent solutions in our experimental condition. Thus, we involved harmonics up to $|n|, |m| = 10$.

III. EXPERIMENTS

We used the electron-beam-lithography method to fabricate the copper nanostrips on (001) Si and amorphous SiO_2 substrates. 5-nm chromium thin film was first deposited for making adhesion strength higher, and then 25-nm copper thin film was deposited. (In the theoretical calculation, we regarded the strip as composed of only copper because of close mass density between chromium (7190 kg/m^3) and copper (8940 kg/m^3).) After lithographic procedures, 499 strip lines remained on the surface with a period d. The length, width w,

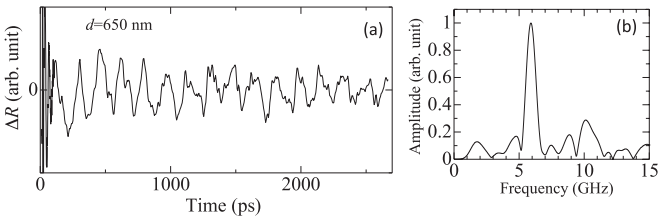

FIG. 2. (a) Reflectivity change of probe light pulse observed for nanostrip specimen with $d = 650$ nm fabricated on the silicon substrate and (b) its Fourier spectrum.

and thickness h of a single strip were 5000, 300, and 30 nm, respectively. We varied the period d between 600 and 1500 nm, making 17 nanostrip specimens on each substrate. Figure 1(c) shows a scanning-electron-microscopy image of the fabricated strip lines with $d = 1000$ nm.

As for the picosecond ultrasound spectroscopy, we used a mode-locking titanium-sapphire pulse laser with 200-fs pulse width. The pump (800 nm, 50 pJ) and probe (400 nm, 50 pJ) light pulses are applied normally at the center area of the nanostrip lines. Diameters of the light pulses are about 80 μm, indicating that nearly 80 strips are excited simultaneously to generate surface waves through the transient thermal expansion, which interfere with each other to cause the standing wave with wavelength close to the strip-line period. The surface-wave resonance is detected by the probe light pulse through its reflectivity change. Details of our optics appear elsewhere [14]. Figure 2(a) shows the typical reflectivity change observed for the nanostrip-attached specimen with $d = 650$ nm on the silicon substrate, which clearly shows the resonance peak near 6 GHz in its Fourier spectrum [Fig. 2(b)].

IV. RESULTS AND DISCUSSION

Figure 3 shows main results in this study. The resonance frequencies were measured with standard deviations smaller than 1% among five independent measurements for all specimens. The measured frequencies (solid circle plots) are significantly lower than the Rayleigh-wave resonance frequencies (frequencies of Rayleigh wave with wavelength d) on the nanostrip-attached silicon at high frequencies, as shown in Fig. 3(a). One may attribute this to the mass-loading effect, because as the period decreases, the volume fraction of the heavier strip increases. For investigating this, we calculated the resonance frequencies based on the mass-loading model proposed previously, where the mass distribution in Eqs. (9) and (10) was considered in the boundary condition for the balance between inertia force caused by the mass and the surface stress [8]. The result is shown with the black solid line. Involving the mass-loading effect, the resonance frequency is lowered, but it is still insufficient to explain the significant frequency decrease at a high-frequency region; the measured frequency is lower by 20% for the smallest-period specimen. More importantly, the resonance frequencies are identical to those of the Rayleigh-wave resonance in the case of the silica substrate [Fig. 3(b)]. In this case, the mass-loading effect should be more noticeable because of lighter substrate. However, the measured resonance frequencies remain nearly

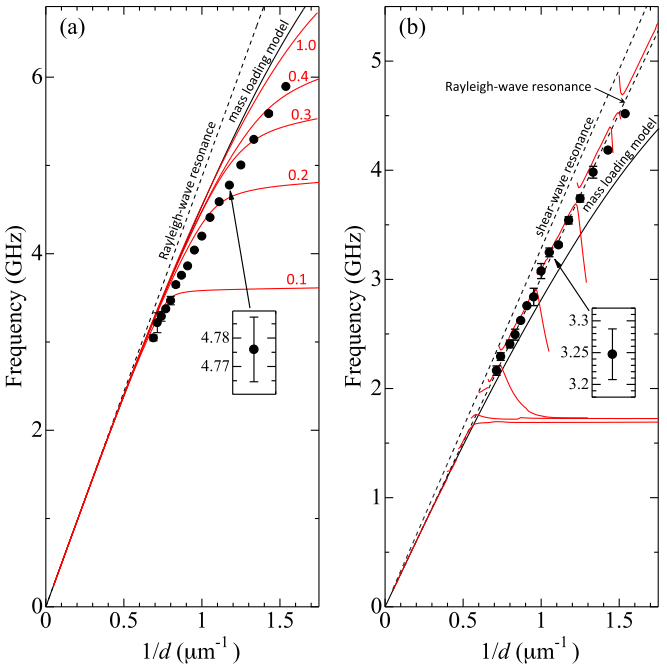

FIG. 3. Relationship between surface-wave resonance frequency and reciprocal period. Solid circles are experiments, and solid black and red lines are calculations with the mass-loading model and the interface-stiffness model in this study, respectively. Broken lines are Rayleigh-wave resonance frequency and shear-wave resonance frequency. (a) Results for silicon substrate. Numbers indicate the p value. (b) Results for silica substrate with $p = 0.01$.

unchanged from the Rayleigh-wave resonance frequencies of the substrate.

Previous studies with finite element methods indicated that the geometrical effect of the strip line could cause significant difference to the mass-loading calculation [15–17], and we investigate its contribution to our experimental results. The duty cycle w/d (or filling fraction) of our specimen is between 0.2 and 0.5, and it increases as the reciprocal period increases. The geometrical effect in this duty-cycle region would increase the frequencies of eigenmodes [15], which fails to explain more significant frequency decrease on the strip-attached silicon than the mass-loading effect [Fig. 3(a)]; the frequency decrease becomes remarkable as the reciprocal period increases. Sadhu *et al.* [16] also indicated that the geometrical effect produced the eigenmode frequencies higher than the mass-loading model, which cannot explain the significant downward shift in Fig. 3(a). (Their calculation always predicted higher frequencies than the mass-loading effect.) The geometrical effect will thus fail to explain both the significant downward frequency shift for the silicon substrate and unchanged frequency for the glass substrate simultaneously. Thus, the previous models cannot reproduce highly decreased frequencies on silicon substrate and nearly unchanged frequencies on silica substrate.

We therefore propose the alternative model involving the interface stiffness. The key is the spring-constant value at the interface [K_1 and K_3 in Fig. 1(a)]. The interatomic bond inside crystalline material is fairly strong compared with the interface bond, and the spring constants per unit area can be

estimated by shear modulus and Young's modulus divided by height of the material for in-plane and out-of-plane directions, respectively. These values are $K_1^{\mathrm{Cu}} = 1.5 \times 10^{18} J/\mathrm{m}^4$ and $K_3^{\mathrm{Cu}} = 4.2 \times 10^{18} \mathrm{J/m}^4$ inside the 30-nm-thick copper nanostrip. The interface spring constant must be much smaller than these values, although they are highly ambiguous. We refer to the bond strength at the grain boundary of polycrystalline material for this, because the grain boundary shows weaker interatomic bonds than the inside crystal [18,19]. Zhang *et al.* [20] calculated the grain-boundary stiffness using a molecular dynamic calculation, from which we estimated the spring constant at the grain boundary to be about $0.4 \times 10^{15} \mathrm{J/m}^4$, and from the calculation by Foiles and Hoyt [21], it is estimated to be $\sim 5 \times 10^{15} \mathrm{J/m}^4$. These values are much smaller than those inside crystal, although their calculations were performed at high temperatures ($>\sim$ 1000 K) and they could be at least one-order higher at room temperature. Then, we introduce a parameter p showing the bond strength at the interface defined as $K_1 = pK_1^{\mathrm{Cu}}$ and $K_3 = pK_3^{\mathrm{Cu}}$ and investigated the surface-wave propagation behavior for $p \geqslant 0.01$. (We assumed the same p value for the two direction stiffness for simplicity, because we find that the contributions on K_1 and K_3 are nearly identical, and this assumption does not affect the principal results in this study.)

Figure 4 shows dispersion relationships for surface waves on the Si substrate with nanostrips of $d = 600$ and 1000 nm when $p = 0.4$. The frequency decreases from that of the Rayleigh wave as the in-plane wave number increases, and this trend becomes more remarkable for smaller d. For $d = 600$ nm, the dispersion relationship shows band gaps not only at the Brillouin-zone boundary at $k_1 = k_B (= \pi/d)$, but also inside the Brillouin zone. Figure 5 shows attenuation changes along the branches indicated by arrows in Fig. 4. Surface-wave attenuation increases as the wave number moves toward the Γ point [$\mathrm{Re}(k_1) = 2k_B$]; this trend becomes remarkable as the strip period becomes smaller. Figure 6 displays the detailed relationship between the dispersion curves and the corresponding attenuation. Very high attenuation occurs near the crossing points with the dispersion lines of bulk waves for the grating with $d = 600$ nm (indicated by arrows), indicating that highly leaky surface waves appear near those points because of the mode coupling into bulk waves.

Because we measure the standing surface-wave resonances, we focus on the Γ-point frequencies for comparing our theory with experiments. Figure 7 shows the relationships between the Γ-point frequency and the reciprocal period with various p values for the Si substrate. It is clearly shown that the resonance frequency significantly decreases and attenuation increases at the high-frequency region as the interface bond weakens. Thus, the high impact of the interfacial stiffness appears in the surface-wave resonance behavior; a drastic frequency decrease could be caused by lowered interface bonds.

As for the silica grass substrate, we assumed a very low interfacial stiffness with $p = 0.01$. This is acceptable because of the lower thermal expansion coefficient of silica, which causes large residual stress at the interface with the metallic (high-thermal-expansion material) strips and induces interfacial defects, leading to highly reduced interfacial stiffness. Actually, this was easily confirmed with ultrasonication of the specimen inside water; ultrasonic irradiation easily caused detachment of the strips from the silica substrate, even with an ultrasonic power, with which strips remained attached on the silicon substrate.

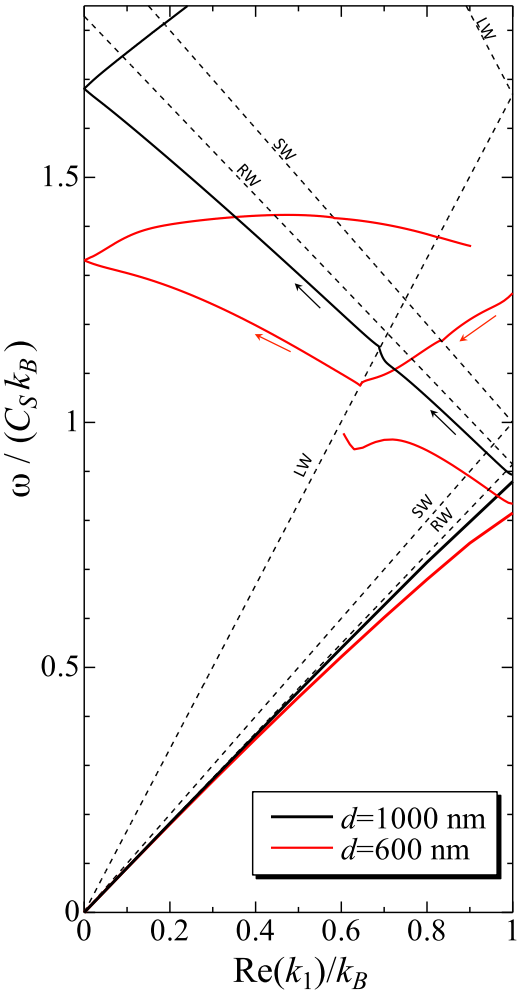

FIG. 4. Dispersion curves calculated for nanostrip specimens with $d = 600$ and 1000 nm on silicon substrate for $p = 0.4$. Broken lines are dispersion curves for Rayleigh wave (RW), longitudinal wave (LW), and shear wave (SW).

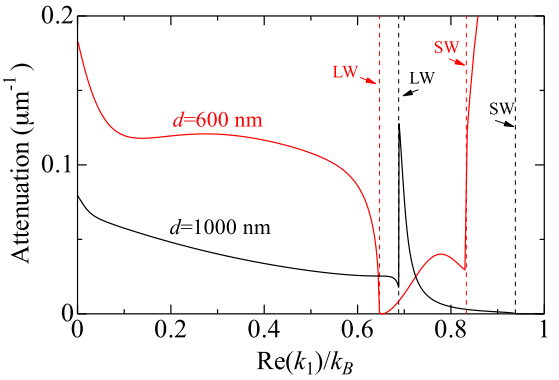

FIG. 5. Attenuation changes along the second branches indicated by arrows in Fig. 4.

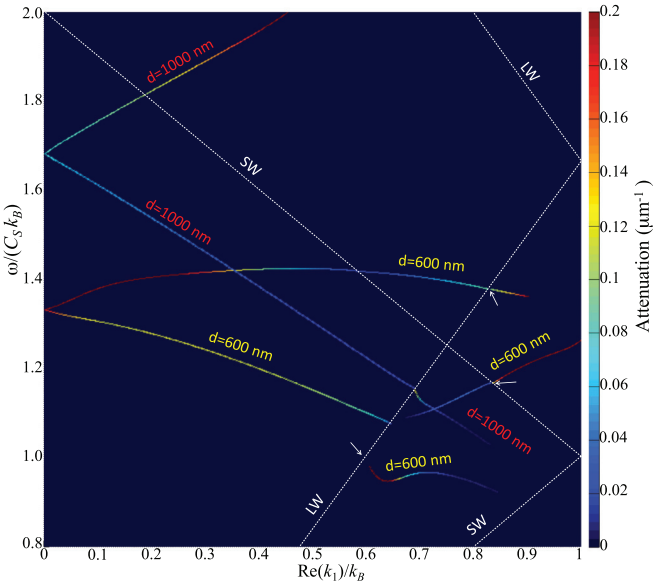

FIG. 6. Dispersion curves with attenuation color gauge for Fig. 4. The white broken lines are dispersion lines for longitudinal wave (LW) and shear wave (SW). Arrows indicate the crossing points between dispersion curves for surface waves and bulk waves, at which highly leaky surface waves occur.

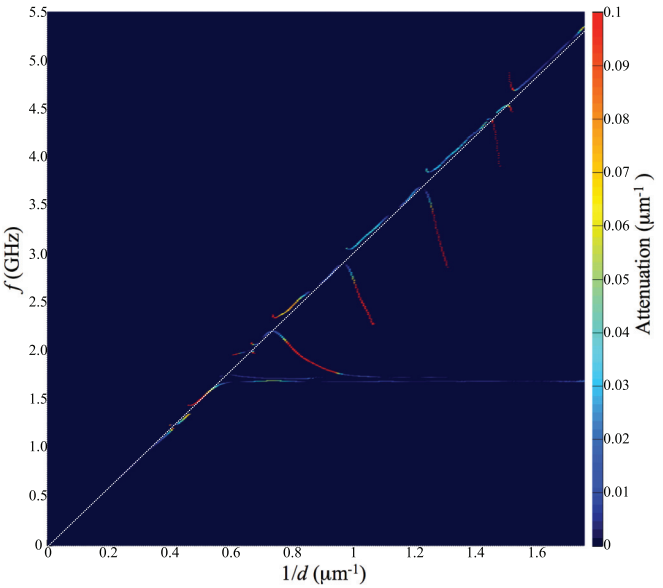

FIG. 8. Relationship between the Γ-point frequency and reciprocal period with attenuation color gauge for silica substrate with $p = 0.01$. The white broken line indicates the Rayleigh-wave resonance.

As shown in Fig. 8, the relationship between the Γ-point frequency and the reciprocal period becomes more complicated for the silica substrate. However, we find that many low-attenuation branches appear along the Rayleigh-wave-resonance line, indicating that the resonance frequencies can be identical to those of the Rayleigh-wave resonance. This trend remains unchanged for other smaller p values (i.e., $p = 0.01$ is not a special case.).

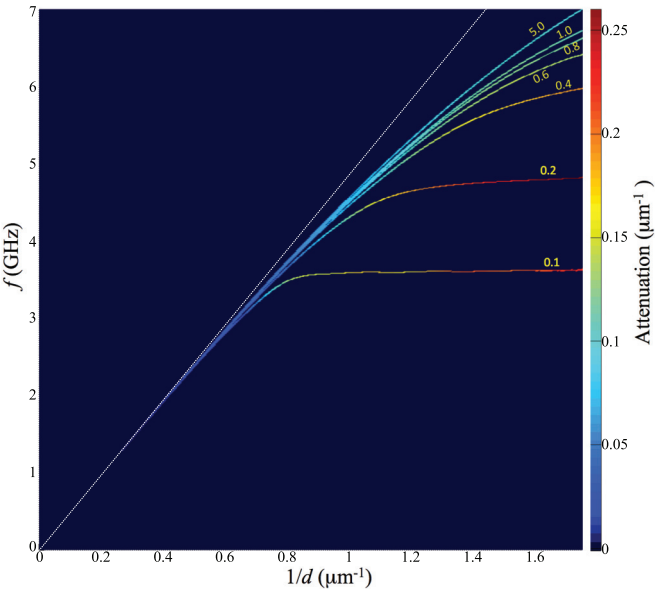

FIG. 7. Relationship between the Γ-point frequency and reciprocal period with attenuation color gauge for silicon substrate with p values between 0.1 and 5.0. The white broken line indicates the Rayleigh-wave resonance.

These calculation results are compared with the experiments in Fig. 3 with solid red lines. For the silicon substrate, our model with $p = 0.4$ explains the depression of the resonance frequency at the high-frequency region, and for the silica substrate, the low interfacial stiffness reproduces the frequencies identical to those of the Rayleigh-wave resonance. Narrow gaps appear in our model [red curves in Fig. 3(b)] and some experimental points lie close to these gaps. However, they are so narrow that the resonance modes on the nearest-neighbor branches will be excited because of certain ambiguity in the strip periods. The low attenuation near the small gaps will also allow the excitation of a nearest-neighbor branch mode.

The essence of these phenomena can be understood with a simple mass-spring oscillator. Consider a series of two mass-spring systems, where a large mass (M) is connected with a rigid wall with a strong spring (spring constant K), and a small mass (m) is connected with the large mass with a soft spring (spring constant k). The large mass and strong spring components correspond to the substrate (the principal oscillator), and the small mass and soft spring components correspond to the added strip with the interface spring in our model. This vibrational system has two resonance frequencies (ω_L and ω_H), and they are easily calculated. Figure 9 shows their changes for various k values. When the interface stiffness k is sufficiently large, the original resonance frequency ($=\sqrt{K/M}$), which corresponds to the Rayleigh-wave resonance frequency in our model, decreases to $\sqrt{K/(M+m)}$, indicating the mass-loading effect. This phenomenon can be confirmed in our model in Fig. 3(a), where as the p value increases the resonance frequency value approaches the prediction by the mass-loading model. As the interface stiffness k decreases, the frequency becomes significantly lower than $\sqrt{K/(M+m)}$ because the overall stiffness decreases; for example, ω can be lower than the

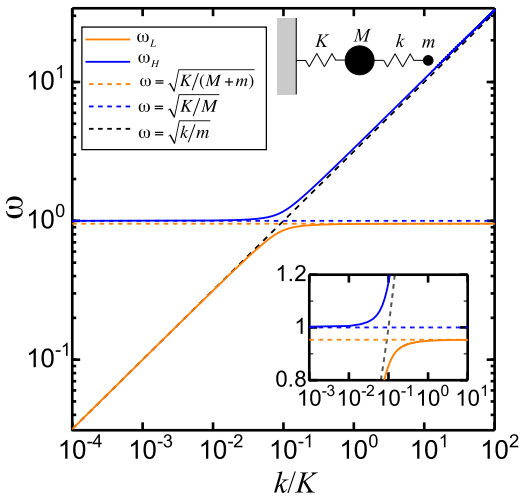

FIG. 9. Resonance frequencies of a two-mass-spring oscillator versus interfacial spring constant k for $K = 1$, $M = 1$, and $m = 0.1$.

original frequency by 20% at $k/K = 0.1$. This corresponds to the case for the silicon substrate. When the interfacial stiffness k becomes very low, for example, $k/K = 0.01$, the principal frequency becomes nearly the same as the original frequency, while the low-frequency mode appears at a very low frequency ($\omega \sim \sqrt{k/m}$). This case will be equivalent to the silica-substrate case, where the system is less sensitive to the added mass because of the very low interfacial stiffness. Low-frequency branches near 1.7 GHz in Fig. 3(b) thus correspond to the low-frequency modes localized at the strips.

V. CONCLUSION

Surface-wave resonances on substrates with periodically aligned nanostrips are systematically studied with picosecond ultrasonic spectroscopy. The strip thickness is only 5% or less than the surface-wave wavelength, but it significantly affects the resonance frequency on the Si substrate; the mass-loading model fails to explain the depression. The frequency decrease was, however, absent on the silica substrate despite a lighter material. The proposed model here, involving the interfacial stiffness between strips and substrate, consistently reproduced these experimental results. Our theoretical model shows that the resonance frequency and attenuation of the surface-wave resonance on strip-attached substrates are highly dependent on the interface bond strength, indicating the necessity of considering the interface stiffness in designing high-frequency surface-wave acoustic resonators.

[1] L. M. Brekhovskikh, Sov. Phys. Acoust. **5**, 288 (1959).
[2] K. Blotekjaer, K. A. Ingebrigtsen, and S. Halvor, IEEE Trans. Electron Devices **20**, 1133 (1973).
[3] Q. Xue and Y. Shui, IEEE Trans. Ultrason. Ferroelectr. Freq. Control **37**, 13 (1990).
[4] A. A. Maznev, Phys. Rev. B **78**, 155323 (2008).
[5] N. E. Glass, R. Loudon, and A. A. Maradudin, Phys. Rev. B **24**, 6843 (1981).
[6] N. E. Glass and A. A. Maradudin, J. Appl. Phys. **54**, 796 (1983).
[7] V. Yantchev, V. Plessky, and I. Katardjiev, J. Appl. Phys. **104**, 034111 (2008).
[8] A. A. Maznev and A. G. Every, J. Appl. Phys. **106**, 113531 (2009).
[9] C. Thomsen, H. T. Grahn, H. J. Maris, and J. Tauc, Phys. Rev. B **34**, 4129 (1986).
[10] O. B. Wright, B. Perrin, O. Matsuda, and V. E. Gusev, Phys. Rev. B **64**, 081202R (2001).
[11] G. A. Antonelli, H. J. Maris, S. G. Malhotra, and J. M. E. Harper, J. Appl. Phys. **91**, 3261 (2002).
[12] H. Ogi, M. Fujii, N. Nakamura, T. Yasui, and M. Hirao, Phys. Rev. Lett. **98**, 195503 (2007).
[13] A. G. Every, Phys. Rev. B **78**, 174104 (2008).
[14] H. Ogi, A. Yamamoto, K. Kondou, K. Nakano, K. Morita, N. Nakamura, T. Ono, and M. Hirao, Phys. Rev. B **82**, 155436 (2010).
[15] D. Nardi, F. Banfi, C. Giannetti, B. Revaz, G. Ferrini, and F. Parmigiani, Phys. Rev. B **80**, 104119 (2009).
[16] J. Sadhu, J. H. Lee, and S. Sinha, Appl. Phys. Lett. **97**, 133106 (2010).
[17] D. Nardi, M. Travagliati, M. E. Siemens, Q. Li, M. M. Murnane, H. C. Kapteyn, G. Ferrini, F. Parmigiani, and F. Banfi, Nano Lett. **11**, 4126 (2011).
[18] H. Ogi, M. Hirao, T. Tada, and J. Tian, Phys. Rev. B **73**, 174107 (2006).
[19] H. Ogi, T. Inoue, H. Nagai, and M. Hirao, Rev. Sci. Instrum. **79**, 053701 (2008).
[20] H. Zhang, D. Du, D. J. Srolovitz, and M. I. Mendelev, Appl. Phys. Lett. **88**, 121927 (2006).
[21] S. M. Foiles and J. J. Hoyt, Acta Mater. **54**, 3351 (2006).